Enhanced Sliding Mode Control for PMSM Speed Drive Systems Using a Novel Adaptive Sliding Mode Reaching Law Based on Exponential Function

Zhang Zhang, Xiaodong Yang, Weiyu Wang, *Student Member, IEEE*, Kaiwen Chen, *Member, IEEE*, Norbert Chow Cheung, *Senior Member, IEEE*, and Jianfei Pan, *Member, IEEE*

***Abstract*—Sliding mode control is widely used to enhance the speed control performance of permanent magnet synchronous motors (PMSM). However, the slow reaching onto the sliding surface and chatting phenomena of conventional sliding mode reaching law (SMRL) is still a challenging issue. This article proposes a novel adaptive SMRL (ASMRL) to solve these problems. This ASMRL includes the system state variables, an exponential function term bounded by the absolute value of the switching function, and an adaptive switching gain term influenced by the convergence of the system state. This approach efficiently accelerates the velocity at which the system state reaches the sliding mode surface and effectively suppresses chattering. Then an enhanced sliding mode controller is designed for the speed regulation of PMSM systems. Finally, mathematical stability analysis, numerical analysis, simulation, and experimental validation are conducted to demonstrate the effectiveness of the proposed method.**

***Index Terms*—Adaptive sliding mode reaching law (ASMRL), exponential function, Lyapunov stability, permanent magnet synchronous motor (PMSM), sliding mode control (SMC), sliding mode reaching law (SMRL).**

I. Introduction

PERMANENT magnet synchronous motors (PMSM) have gained significant attention and widespread adoption due to their high-power density, efficiency, low inertia, and excellent dynamic response characteristics [1]. Sliding mode control (SMC) has garnered significant attention as a widely applied nonlinear method for controlling PMSMs [2], [3], [4], [5], [6], [7], [8], [9], [10]. SMC offers several advantages, including its robustness against model inaccuracies and nonlinearities. This type of algorithm does not rely heavily on precise system models, making it suitable for many practical applications. As a result, SMC has been successfully applied in various servo systems [6].

Design SMC with sliding mode reaching laws (SMRLs) is a typical method for SMC. Due to its convenient design and computational aspects, it has been extensively studied in recent years [11], [12], [13]. Gao was the first to propose and utilize the concept of reaching law [14]. The role of the reaching law is to drive the state trajectories to reach a designed sliding surface within a finite time. However, conventional SMRLs can exhibit the phenomenon of slow reaching, whether the system is near or far from the sliding surface [15]. In practical applications, this can result in poorer dynamic performance and reduced disturbance rejection capability.

To accelerate the reaching process of this method, in [16] a suitable SMC law that achieves the SMC reaching process within a specified finite time interval based on finite-time boundedness for a certain class of nonlinear systems. In [17], a new SMRL is designed that incorporates the state variable and is influenced by the absolute value of the sliding switching function. This reaching law exhibits two different forms, each with distinct characteristics. An improved exponential reaching law (ERL) is employed to accelerate the reaching process within a fractional-order SMC strategy in [18]. In addition to this method, there are also SMC design approaches that combine with other algorithms to accelerate the reaching process. In [19] a two-stage switching hybrid control method utilizing an enhanced particle swarm optimization approach, it preserves the quick response of SMC, but it might pose challenges in terms of implementation within certain practical systems or involves complex parameter tuning and other challenges [20].

Another main drawback of SMC design with SMRL methods is the occurrence of chattering, which is caused by the discontinuous control law and the frequent switching near the sliding surface [14]. Since the control law is derived from the employed

Manuscript received 11 September 2023; revised 29 November 2023; accepted 16 December 2023. This work was supported in part by the National Natural Science Foundation of China under Grant 52277060 and Grant U1913214 and in part by General Research Project of Shenzhen Science and Technology Plan under Grant JCYJ20220818100000001. *(Corresponding author: Jianfei Pan.)*

The authors are with the College of Mechatronics and Control Engineering, Shenzhen University, Shenzhen 518061, China (e-mail: zhangzhang2022@email.szu.edu.cn; yangxiaodong2021@email.szu.edu.cn; weiyu.wang@connect.polyu.hk; kwchen@szu.edu.cn; norbertcheung@szu.edu.cn; pjf@szu.edu.cn).

Color versions of one or more figures in this article are available at https://doi.org/10.1109/TIE.2023.3347845.

Digital Object Identifier 10.1109/TIE.2023.3347845

reaching law, the design of the reaching law plays a significant role in mitigating the chattering effect and reducing the reaching time [21]. This undesirable chattering phenomenon can lead to high-frequency noise signals and significant steady-state errors and limits the practicality and effectiveness of SMC in practical applications. A direct approach to address the chattering issue is to replace the sign function with a continuous switch function [15], mitigating the chattering issue by employing a control law with continuous variations. Another method involves reducing the switching gain to minimize chattering [13], however this type of method also has its limitations, reducing the switching gain to mitigate chattering may lead to increased reaching time on the sliding surface. Therefore, when selecting the gains in the reaching laws, a compromise often needs to be made between the chattering amplitude and reaching time [21].

To address the inherent contradiction between accelerating the SMC reaching process and mitigating the chattering phenomenon, this article proposes an adaptive sliding mode reaching law (ASMRL) based on the exponential function and existing SMRL. The exponential function, widely recognized for its rapid growth, proves effective in reducing the reaching time when applied to the design of SMRL. This ASMRL incorporates system state variables, an exponential term bounded by the absolute value of the switching function, and an adaptive switching gain term influenced by the convergence of system states, can effectively accelerates the SMC reaching process and suppresses chattering. Based on the designed novel ASMRL, a SMC method was developed to enhance the speed control performance of PMSM. The results demonstrate the superiority and effectiveness of the proposed approach.

The contributions of the article are highlighted as follows.

1) A novel ASMRL is designed, which exhibits some characteristics of conventional SMRL while enhancing its performance, this improvement helps accelerate the SMC reaching process and reduce chattering in conventional SMRL. This method is proposed to address the inherent contradiction between accelerating the SMC reaching process and mitigating the chattering phenomenon.
2) For the problem of designed SMRL, most of the newly designed SMRL may have implementation challenges due to it difference from conventional SMRL. The ASMRL designed in this article exhibits some characteristics of conventional SMRL and can be directly applied to SMC systems to enhance their performance without additional implementation problems.

II. Design and Analysis of the ASMRL

A. Design of the ASMRL

In this section, a novel ASMRL based on the exponential function and existing SMRL is proposed, analyzing the design steps and performance. It exhibits some characteristics of ERL and the terminal sliding mode reaching law (TSMRL).

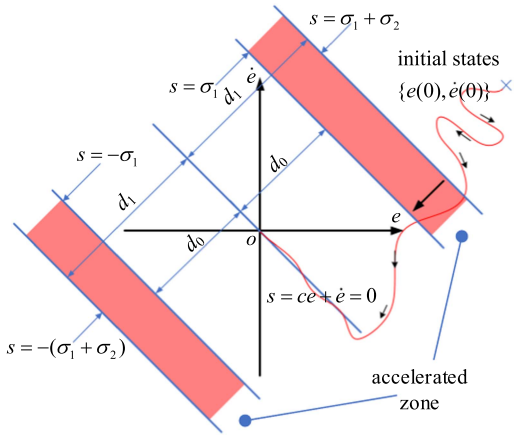

Fig. 1. SMC process with '$-k_2(e^{bo}-1)\mathrm{sgn}(s)$' term.

The following second-order nonlinear model is widely employed to describe SMC systems that utilize reaching law methods. Assume a second-order nonlinear model

$$\ddot{\theta}(t) = -f(\theta,t) - g(t) + bu(t) \tag{1}$$

where $\theta(t)$ is the system position, $g(t)$ represents the system disturbances, b is not equals to zero, and $u(t)$ is the input of controller. $x=[x_1,x_2]^T$ is the state variable, defined x_1 as the tracking error, namely $\theta_i-\theta$. θ_i represents reference position

$$\begin{cases} x_1 = e = \theta_i - \theta \\ x_2 = \dot{x}_1 = \dot{e} = \dot{\theta}_i - \dot{\theta} \end{cases}. \tag{2}$$

A typical sliding function is chosen as follows:

$$s = cx_1 + x_2 \tag{3}$$

where $c>0$ can satisfy the Hurwitz condition. Such sliding mode surface ($s=0$) can guarantee the asymptotic stability of the sliding mode. The ASMRL can be described as follows:

$$\begin{aligned} \dot{s} = & -\xi\mathrm{sgn}(s)\left(\frac{E}{E+d}\right)(1+k_3|x_2|) - k_0 s \\ & - k_1|s|^a E^n \mathrm{sgn}(s) - k_2(e^{bE}-1)\mathrm{sgn}(s)\cdot X \end{aligned} \tag{4}$$

where, $\xi>0, k_1>0, k_2>0, k_3>0, b>0, 0<a<1, 0<n<1, 0<a+n<1, \sigma_1>0, \sigma_2>0$, and d is a positive constant and its value is considered with respect to E. x is the state variable of the system error ($x\in R_n$). The term E represents the Euclidean distance in state space between equilibrium point and current position

$$E = \sqrt{x_1^2 + x_2^2 + \ldots x_n^2} \tag{5}$$

when the sliding state is far away from the desired trajectory, the $-k_2(e^{bE}-1)\mathrm{sgn}(s)$ term becomes the dominant factor in driving the state trajectories towards the sliding surface.

However, the exponential growth rate may sometimes lead to undesirable effects. To mitigate the undesired effects, it is limited to operate within specific regions: "accelerated zone." Four state surfaces parallel to the sliding surface ($s=0$) are used to establish the accelerated zone. Fig. 1 demonstrates the

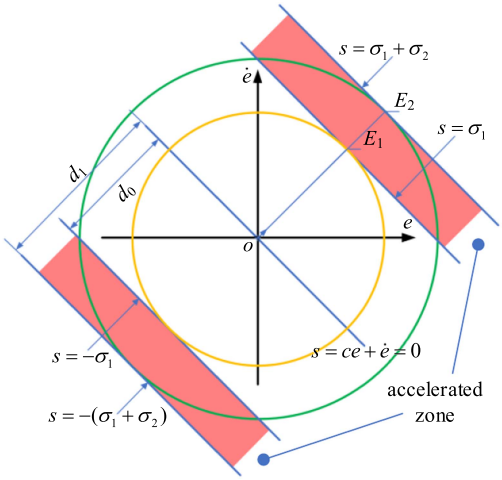

Fig. 2. Geometry relationship between σ_1, σ_2, and E.

reaching process of the sliding state toward the sliding trajectory with the $-k_2(e^{bE}-1)\mathrm{sgn}(s)$ term.

$(\sigma_1| < |s| < \sigma_1+\sigma_2)$ is also the condition for determining

$$X=\begin{cases}1, \sigma_1<|s|<\sigma_1+\sigma_2\\ 0, \text{else}\end{cases}. \tag{6}$$

In Fig. 1 d_0, d_1, can consider as the distance between sliding-mode surface and other parallel surface based on the geometric equation

$$\frac{\sigma_1}{\sqrt{1+c^2}}=d_0, \frac{\sigma_1+\sigma_2}{\sqrt{1+c^2}}=d_1. \tag{7}$$

The value of σ_1, σ_2 based on the equation as follow (7), when $|k_2(e^{bE}-1)\mathrm{sgn}(s)|\le\xi$, the $-k_2(e^{bE}-1)\mathrm{sgn}(s)$ term of ASMRL no longer plays a dominant role. At these states (represented by the yellow circle in Fig. 2), where $E=E_1=d_0$, select the state with the maximum $|s|$ to set σ_1, E_1 based on the condition

$$\left|k_2(e^{bE_1}-1)\mathrm{sgn}(s)\right|=\xi\rightarrow E_1=\frac{1}{b}\ln\left(\frac{\xi}{k_2}+1\right). \tag{8}$$

Then the geometry relationship between σ_1 and $E_1=d_0$ (7)

$$\sigma_1=E_1\sqrt{1+c^2}=\frac{\sqrt{1+c^2}}{b}\ln\left(\frac{\xi}{k_2}+1\right). \tag{9}$$

To ensure a smoother reaching process and a minimum unnecessary disturbance. the saturation function is employed to restrict the dominant influence of the $-k_2(e^{bE}-1)\mathrm{sgn}(s)$ term in the ASMRL. The maximum output of the saturation function is determined based on the system characteristics and the practical application requirements

$$\begin{aligned}&\left|-k_2(e^{bE}-1)\mathrm{sgn}(s)\right|\le|\max(\mathrm{sat})|\\ &\text{when}: E=E_2, k_2(e^{bE_2}-1)=|\max(\mathrm{sat})|\end{aligned} \tag{10}$$

$|\max(\mathrm{sat})|$ represent the upper limit of saturation function. Fig. 2 demonstrates the geometry relationship between σ_1, σ_2 and E. The yellow circle and green circle represent the states where $E = E_1$ and $E = E_2$, respectively. Since $d_1 = E_2$, according to (7)

$$\sigma_1+\sigma_2=E_2\sqrt{1+c^2}=\frac{\sqrt{1+c^2}}{b}\ln\left[\frac{|\max(\mathrm{sat})|}{k_2}+1\right]. \tag{11}$$

By substituting (9) into (11), and by assuming that the value of $|\max(\mathrm{sat})|$ is much larger than k_2 and ξ, it can express σ_2 in a form as shown in (12). Considering the practical considerations; for the purpose of simplification, set σ_2 to be the value described in the inequality

$$\begin{aligned}&\frac{\sqrt{1+c^2}}{b}\ln\left\{\left[\frac{|\max(\mathrm{sat})|}{k_2}+1\right]-\ln\left(\frac{\xi}{k_2}+1\right)\right\}\\ &=\frac{\sqrt{1+c^2}}{b}\ln\left[\frac{|\max(\mathrm{sat})|+k_2}{\xi+k_2}\right]>\frac{\sqrt{1+c^2}}{b}\ln\left[\frac{|\max(\mathrm{sat})|}{\xi+k_2}\right].\end{aligned} \tag{12}$$

Considering the above, the value of σ_2 can be determined, with the accelerated zone adopting the values in (9) and (13)

$$\sigma_2=\frac{\sqrt{1+c^2}}{b}\ln\left[\frac{|\max(\mathrm{sat})|}{\xi+k_2}\right]. \tag{13}$$

For the term $-\xi\mathrm{sgn}(s)[E/(E+d)](1+k_3|x_2|)$, when the sliding state is away from the sliding trajectory, the term $[E/(E+d)]$ approximates to 1. As E approaches zero, the value of $[E/(E+d)]$ decreases and eventually becomes zero. On the other hand, $(1+k_3|x_2|)$ is introduced to mitigate the lumped disturbances. x_2 represents the time derivative of the tracking error, and k_3 is a small constant compared to other parameters. If there are no disturbances causing variation in the tracking error, the value of $(1+k_3|x_2|)$ approximates to 1. However, if the system is disturbed, then the term $(1+k_3|x_2|)$ increases, due to this reason the value of $(1+k_3|x_2|)$ will also increase to suppress the disturbances.

For the $-k_1|s|^aE^n\mathrm{sgn}(s)$ term is modified by TSMRL [7] to plays an intermediate role in the SMC process, when the sliding state is inside or outside the accelerated zone, it may cause disturbances due to the variations of $\dot{s}$. This term is introduced to mitigate the sliding state variation caused by $\dot{s}$. In this condition, the SMC can enhance the reaching velocity of the sliding state variable and significantly reduce the chattering phenomenon.

B. Convergence Time Analysis of the ASMRL

The convergence time of the reaching law can be derived from (4). With $s(t)=0$, s_0 represents the value of the $s(x)$ of initial states ($|s_0|>\sigma_1+\sigma_2>0$). represents the time taken to reach sliding surface ($s=0$) from any initial states [8].

The numerical values in the expression can be simplified. The convergence time of ASMRL is subsequently formulated

$$t<\int_{|s_0|}^{\sigma_1+\sigma_2}\frac{1}{\dot{s}_1}ds+\int_{\sigma_1+\sigma_2}^{\sigma_1}\frac{1}{\dot{s}_2}ds+\int_{\sigma_1}^{0}\frac{1}{\dot{s}_1}ds. \tag{14}$$

Since the $-k_2(e^{bE}-1)\mathrm{sgn}(s)$ term plays a significant role in the accelerated zone, $\dot{s}_1$and $\dot{s}_2$ can be simplified as

$$\dot{s}_1=\left|-k_0s-k_1|s|^aE^n\mathrm{sgn}(s)\right|;\dot{s}_2=\left|-k_2(e^{bE}-1)\mathrm{sgn}(s)\right|. \tag{15}$$

According to Fig. 2 and the geometry relationship of E and s

$$E = \sqrt{x_1^2 + x_2^2} \geq \frac{|cx_1 + x_2|}{\sqrt{1+c^2}} = \frac{|s|}{\sqrt{1+c^2}}. \tag{16}$$

Therefore, according to (16), the (15) can express as inequality can be obtained as

$$\dot{s}_1 \geq \left| k_0 s + k_1 (1+c^2)^{-\frac{n}{2}} |s|^{a+n} \right|, \dot{s}_2 \geq \left| k_2 (\mathrm{e}^{\frac{bs}{\sqrt{1+c^2}}} - 1) \right|. \tag{17}$$

By calculating the definite integral on the right side of the inequality in (15), The final expression for the convergence time can be obtained as

$$\begin{aligned} t < {} & \Delta_2 \ln \left[\left(\frac{k_0 |s_0|^{1-a-n}}{\Delta_1} + 1 \right) \left(\frac{k_0 \sigma_1^{1-a-n} + \Delta_1}{k_0 (\sigma_1 + \sigma_2)^{1-a-n} + \Delta_1} \right) \right] \\ & + \frac{\Delta_3}{k_2} \ln \left(\frac{e^{\frac{\sigma_1}{\Delta_3}} - e^{-\frac{\sigma_2}{\Delta_3}}}{e^{\frac{\sigma_1}{\Delta_3}} - 1} \right) \leq \Delta_2 \ln \left(\frac{k_0 |s_0|^{1-a-n}}{\Delta_1} + 1 \right). \end{aligned} \tag{18}$$

The symbols defined in (18) are represented as follows:

$$\Delta_1 = k_1 (1+c^2)^{-\frac{n}{2}}, \Delta_2 = \frac{1}{k_0 (1-a-n)}, \Delta_3 = \frac{\sqrt{1+c^2}}{b}. \tag{19}$$

Consider the case where σ_2 equals to zero, indicating the absence of accelerated zone, or $|s_0| < \sigma_1$. In these cases, the inequality becomes an equality, implying that the system state requires more convergence time. The analysis of convergence time means that the system state can reach the equilibrium state in a finite time from any initial state.

C. Numerical Analysis of the ASMRL

The performances of the ERL [6], TSMRL [7], and ASMRL can be compared by the numerical analysis method. First, a second-order nonlinear model is established using (20) for analysis, where $\theta(t)$ is the position, $g(t)$ represents the system disturbances, $u(t)$ is the input of controller

$$\ddot{\theta}(t) = -25\dot{\theta} - g(t) + 133u(t). \tag{20}$$

Here, θ_i is the reference signal, $\theta_i = \sin(t)$, The tracking error of the position θ and its derivative can be written as (2), Based on (3) and considering (4)

$$\begin{aligned} \dot{s} &= c\dot{x}_1 + \dot{x}_2 = c(\dot{\theta}_i - \dot{\theta}) + (\ddot{\theta}_i - \ddot{\theta}) \\ &= -\xi \mathrm{sgn}(s) \left(\frac{E}{E+d} \right) (1 + k_3 |x_2|) - k_0 s \\ &\quad -k_1 |s|^a E^n \mathrm{sgn}(s) - k_2 (\mathrm{e}^{bE} - 1) \mathrm{sgn}(s) \cdot X. \end{aligned} \tag{21}$$

By substituting (20) into (21) the control input $u(t)$ as

$$\begin{aligned} u(t) = \frac{1}{133} [& \xi \mathrm{sgn}(s) \left(\frac{E}{E+d} \right) (1 + k_3 |x_2|) + k_0 s \\ & + k_1 |s|^a E^n \mathrm{sgn}(s) + k_2 (\mathrm{e}^{bE} - 1) \mathrm{sgn}(s) \cdot X \\ & + c x_2 - \sin(t) + g(t) + 25\dot{\theta}]. \end{aligned} \tag{22}$$

In the numerical analysis, the motor model is simulated by using the s-function in MATLAB for the ERL, TSMRL, and ASMRL approaches. The parameter values are set as follows: $\xi = 5$, $a = 0.5$, $b = 1.5$, $c = 1.5$, $d = 2$, $k_0 = 30$, $k_1 = 1$, $k_2 = 10$, $k_3 = 0.05$, $n = 0.2$, $\sigma_1 = 0.05$, $\sigma_2 = 3.5$. The initial state is set as $x = [x_1, x_2]^T = [-0.15, -0.15]$. Fig. 3 illustrates the performance of the ERL, TSMRL, and ASMRL.

Through numerical analysis, a comprehensive comparison can be obtained. Fig. 3(a) illustrates that the ASMRL exhibits quicker response dynamics and reduced chattering. Fig. 3(b) reveals that the ASMRL achieves smaller tracking error and quicker tracking response. Based on the observations from Fig. 3, it can be concluded that the ASMRL presents better tracking capability, faster reaching process and diminished chattering, when compared to ERL and TSMRL methods.

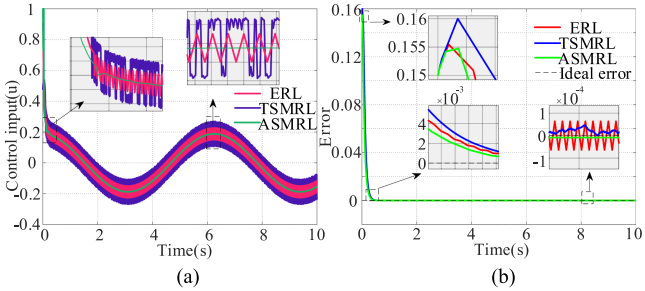

Fig. 3. Numerical performance comparison. (a) Control input. (b) Position tracking error.

III. Design of Sliding Mode Control of the PMSM Based on the ASMRL

A. Dynamic Model of the PMSM

The dynamic model of the PMSM can be expressed as

$$\begin{cases} \frac{di_d}{dt} = \frac{1}{L_d} (u_d - R_s i_d + L_q n_p \omega i_q) \\ \frac{di_q}{dt} = \frac{1}{L_q} (u_q - R_s i_q - L_d n_p \omega i_d - n_p \omega \psi_f) \\ \frac{d\omega}{dt} = \frac{1}{J} (1.5 n_p \psi_f i_q - B\omega - T_L) \end{cases} \tag{23}$$

where is n_p the number of pole pairs, ψ_f is the permanent magnet flux linkage, J, T_L, and B are the moment of inertia, load torque and damping coefficient, u_d, u_q, i_d, and i_q are the d–q axis stator voltages and currents, and R_s and L_s are the stator resistance and inductance, respectively.

B. Enhanced Sliding Mode Speed Control of the PMSM Based on the ASMRL

The motor speed error and is its derivative chosen as the main variable for designing the sliding mode controller, where ω^* and ω are the reference and actual speeds

$$\begin{cases} x_1 = \omega^* - \omega = e \\ x_2 = \dot{x}_1 = \dot{\omega}^* - \dot{\omega} = \dot{e} \end{cases}. \tag{24}$$

According to (23) and substituting into (24), it can obtain

$$\dot{e} = \dot{\omega}^* - \dot{\omega} = \dot{\omega}^* + \frac{1}{J} \left(T_L + B\omega - \frac{3}{2} n_p \psi_f i_q \right). \tag{25}$$

The output of the speed controller i_q^* can be obtained through (25). To further reduce chattering in the SMC, a sigmoid function is utilized as a replacement for the sign function, ρ is a constant that can be modified

$$\mathrm{sigmoid}(s) = \frac{2}{\mathrm{e}^{-\rho s} + 1} - 1. \tag{26}$$

The final output of the speed control based on ASMRL can be derived by (3), (4), (24), and (25)

$$u(t) = \frac{1}{C}\{\int_0^t [\xi \text{sigmoid}(s)(\frac{E}{E+d})(1+k_3|x_2|) + k_0 s + k_2(e^{bE}-1)\text{sigmoid}(s)\cdot X + k_1|s|^a E^n \text{sigmoid}(s)]dt + cx_1 + \dot{\omega}^* + D(t)\}. \quad (27)$$

In the expression (27), C represents the $(3n_p\psi_f)/2J$, $D(t)$ which represents the lumped disturbances including $(T_L + B\omega)/J$, and suppose $l \geq 0$ which is the disturbances bound, $|D(t)| \leq l$. In the following content, E-SMC is used to represented Enhanced SMC. In addition, the traditional SMC in this article refers to the SMC designed based on the ERL using the Section III-B method.

C. Stability Proof of the Enhanced Sliding Mode Controller

To verify whether the design of the E-SMC speed controller can drive the speed error of the PMSM to converge to 0 within a finite time in an asymptotic manner, the stability of the system can be analyzed using the Lyapunov function. The Lyapunov function can be defined as follows:

$$V = \frac{1}{2}s^2. \quad (28)$$

To ensure that the system satisfies the sliding-mode reaching condition, which is expressed as follows:

$$\dot{V} = \dot{s}s \leq 0. \quad (29)$$

Substituting (3), (24) and (25) into (30)

$$\dot{V} = s\dot{s} = s(c\dot{e} + \ddot{e}) = s\left\{c\dot{e} + \ddot{\omega}^* + \frac{d}{dt}\left[\frac{1}{J}(T_L + B\omega - \frac{3}{2}n_p\psi_f u(t))\right]\right\}. \quad (30)$$

Substituting (27) into (30), and consider $X \leq 1$

$$\dot{V} \leq -\xi \text{sgn}(s)s(\frac{E}{E+d})(1+k_3|x_2|) - k_0 s^2 - k_1|s|^a E^n \text{sgn}(s)s = -f(x,E,s) - k_0 s^2, (x \in R^n, E \in R, s \in R). \quad (31)$$

The $f(x, E, s)$ can be written as

$$f(x,E,s) = \text{sgn}(s)s\left[\xi\left(\frac{E}{E+d}\right)(1+k_3|x_2|) + k_1|s|^a E^n\right]. \quad (32)$$

Since $\text{sgn}(s)s = |s|$, and the value of parameters

$$\xi > 0, E > 0, d > 0, k_3 > 0 \Rightarrow \xi(\frac{E}{E+d})(1+k_3|x_2|) > 0$$
$$k_1 > 0, 0 < a < 1, 0 < n < 1, 0 < n+a < 1 \Rightarrow k_1|s|^a E^n > 0. \quad (33)$$

Due to the algebraic relation of (33), (32) can be expressed as

$$f(x,E,s) = |s|\left[\xi\left(\frac{E}{E+d}\right)(1+k_3|x_2|) + k_1|s|^a E^n\right] > 0. \quad (34)$$

Furthermore, substituting (28) into (31) and considering the inequality relation of (34), (31) can be further expressed as

$$\dot{V} = -f(x,E,s) - k_0 s^2 = -f(x,E,s) - 2k_0 V \leq -2k_0 V. \quad (35)$$

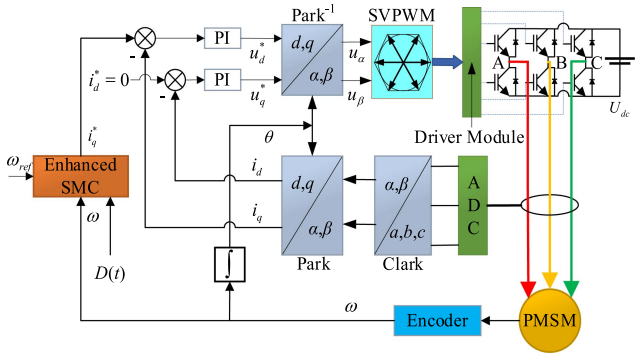

Fig. 4. Block diagram of the PMSM speed regulation system.

It is guaranteed that all terms of (35) are smaller than zero. The time-domain solution of the Lyapunov function is given by

$$V(t) = e^{-2k_0(t-t_0)}V(t_0) + \int_{t_0}^{t} e^{-2k_0(t-\tau)}[-f(\tau)]\,d\tau. \quad (36)$$

For the Lyapunov function $V(t)$: $[0,\infty) \in R$, $t > t_0$

$$\text{since}: f(x,E,s) = f(t) > 0 \Rightarrow \int_{t_0}^{t} e^{-2k_0(t-\tau)}[-f(\tau)]\,d\tau < 0$$
$$V(t) \leq V(t_0)\,e^{-2k_0(t-t_0)}. \quad (37)$$

Clearly as shown, $V(t)$ will exponentially converge to zero. The convergence speed depends on k_0 and other parameters in ASMRL. The Lyapunov stability condition is fully satisfied. Therefore, it can be concluded that the state variables of the system will converge to zero within a finite time.

IV. Simulation and Experiment Results

The vector control strategy of $i_d^* = 0$ is utilized to decouple the speed and currents. The control structure of the PMSM speed regulation system based on the proposed E-SMC method is shown in Fig. 4.

A. Simulation Verification

To verify the effectiveness of the proposed E-SMC method, a simulation is conducted and compared with traditional SMC, and PI controller [27]. The parameters of the PMSM used in the simulation are given in Table I. Based on the analysis from the above section, the parameters of the proposed sliding mode controller are $\xi = 50$, $a = 0.22$, $b = 0.0005$, $c = 120$, $d = 200$, $k_0 = 1500$, $k_1 = 1000$, $k_2 = 3000$, $k_3 = 0.0001$, $n = 0.41$, $\sigma_1 = 1500$, and $\sigma_2 = 60000$. Simulation verification is conducted with variations in ξ, k_2, and b, where the values of σ_1 and σ_2 follow the constraints given in (9) and (13). The simulation results involve the PMSM operating at speeds ranging from 0 to 300 r/min. At 0.2 s, adding a 2 N·m load torque to the PMSM system. To highlight the comparative effects, the output of each controller was elevated with appropriate gain values.

1) From Fig. 5, the variations in σ_1 and σ_2 are influenced by the change in the ξ value. When $\xi = 500$, the controller does not effectively accelerate the approaching process, and the overshoot is close to that of the traditional SMC.

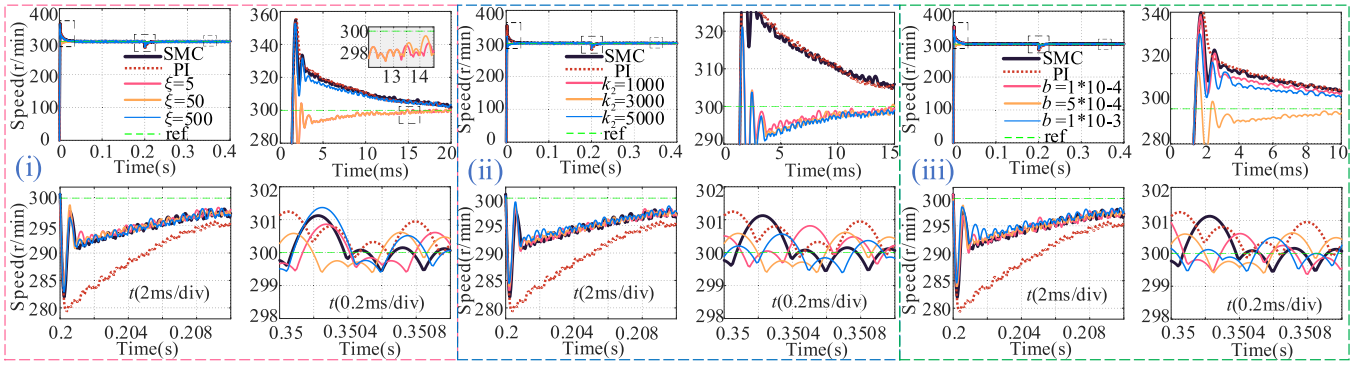

Fig. 5. Speed responses under PI, SMC and E-SMC with different values of the parameters, (i), (ii), and (iii).

TABLE I
MAIN PARAMETERS OF THE SIMULATION SETUP

Symbol	Parameters	Value
n_p	Pole pairs	4
ψ_f	Flux linkage	0.09 Wb
R_s	Stator resistance	0.8 Ω
L_s	d–q axis inductances	5.0*10^{-3} H
J	Inertia of motor	1.59*10^{-4} kg·m^2
B	Viscous damping	2.0*10^{-5} N·m·s /rad
T_s	Sample time	1.0*10^{-5} s
T_{pwm}	Switching time	1.0*10^{-4} s
U_{dc}	DC voltage	311 V
k_p	Proportional	25 Hz
k_i	Integral	4000 Hz

This is because the large ξ value leads to an increase in the theoretical value of σ_1, causing the initial state of $|s|$ to be already smaller than σ_1, thus failing to achieve effective acceleration. Indeed, both $\xi = 5$ and $\xi = 50$ can effectively accelerate the system, resulting in significantly reduction of overshoot and settling time. From the load response, it can be observed that the variation of ξ did not significantly affect the speed drop in the E-SMC. Additionally, at 0.2 s, then the system states have already converged, and they are not located within the accelerated zone. Therefore, at this point, the speed response of the E-SMC is only slightly better than the SMC. From the steady-state response at 0.35 s, it can be observed that, as the value of ξ increases, the speed fluctuations become more pronounced due to the increased chattering.

2) From Fig. 5, it can be observed that, although the variation of k_2 affects the values of σ_1 and σ_2, the designed accelerated zone is still within a suitable range for the initial state of the system. Due to the dominant role of the designed exponential function term within the accelerated zone, the speed response curves of E-SMC with different k_2 values are quite similar, with reduced overshoot and settling time.
3) From Fig. 5, it can be observed that the variation of parameter "b" leads to changes in σ_1 and σ_2. When $b = 1*10^{-4}$, the acceleration is not successful due to a large variation in σ_1. On the other hand, when $b = 1*10^{-3}$, the issue arises from σ_2 being too small. $\sigma_1 + \sigma_2$ indicates the value of $|s|$ at the far end of the acceleration zone from the equilibrium point. The failure to achieve successful acceleration during the period with the largest state error is due to the initial state being located too far away from the accelerated zone.

Based on (9) and (13), it can adjust the acceleration zone by appropriately broadening it. Exactly, the goal is to ensure that the state with relatively large error after the initial state remains within the accelerated zone. In addition, it is important to select a suitable value for ξ to prevent significant chattering phenomena. To quantitatively validate the performance of the proposed method, using various indexes, such as root mean square (RMS), overshoot, and speed drop [3]. where Ns is the number of the samples

$$\mathrm{Rms}(e) = \sqrt{\sum_{i=1}^{N_s} \frac{e^2(i)}{N_s}}. \tag{38}$$

Table II gives the simulation data indexes from Fig. 5(i)–(iii). It can be observed the numerical values of various indexes for the E-SMC are consistently lower when compared to those of traditional SMC. Based on the magnitude of the RMS and speed drop, It is evident that the settling time of E-SMC is consistently smaller than that of SMC. By selecting appropriate parameter combinations, E-SMC can achieve better dynamic and steady-state performances.

To validate the robustness of the of E-SMC, comparative simulation were designed based on different system parameters. The controller parameters were set as Table II for E-SMC and SMC, with $J_0 = 1.59*10^{-4}$ kg·m^2, $\psi_0 = 0.09$ Wb, T_L ranging from 2 to 4 N·m. Table III reveals that the performance of the system exhibits insensitivity to variations in system parameters. This highlights the strong robustness of SMC and it reflects the improved robustness of E-SMC compared to SMC.

In order to analyze the impact of $(1 + k_3|x_2|)$ on the system performance and obtain more pronounced comparative results, the majority of the PMSM system's parameters and controller parameters were consistent with those presented in Tables I and II. The ideal current loop model was employed, with the

TABLE II
PERFORMANCE COMPARISONS OF CONTROLLERS

Controller	RMS Speed (r/min)	RMS Load (r/min)	Over-shoot (r/min)	Speed Drop (r/min)
ξ=5 σ_1 = 400, σ_2 = 60000	16.3609	1.3637	21.1205	15.4792
ξ=50 σ_1 = 1500, σ_2 = 60000	16.3611	1.3746	21.1205	16.0267
ξ=500 σ_1 = 37000, σ_2 = 60000	16.7580	1.4414	52.7262	17.0928
k_2=1000 σ_1 = 11000, σ_2 = 70000	16.3428	1.4287	21.1205	16.7879
k_2=3000 σ_1 = 1500, σ_2 = 60000	16.3611	1.3746	21.1205	16.0267
k_2=5000 σ_1 = 2500, σ_2 = 60000	16.3683	1.3036	21.1205	15.5357
b=1*10^{-4} σ_1 = 20000,σ_2 = 180000	16.7492	1.4329	52.7262	16.0111
b=5*10^{-4} σ_1 = 1500, σ_2 = 60000	16.3611	1.3746	21.1205	16.0267
b=1*10^{-3} σ_1 = 2000, σ_2 = 18000	16.5892	1.2332	42.6392	15.3945
SMC: k_0=1500, ξ=50	16.9566	1.4624	54.8438	18.0418
PI: k_p=0.02, k_i =3.10	17.0442	2.7005	55.5029	20.6372

TABLE III
PERFORMANCE COMPARISONS OF PARAMETERS

Parameters	E-SMC			SMC		
	A	B	C	A	B	C
$J = J_0$	21.12	16.02	5.61	54.84	18.04	16.20
$J = 1.5J_0$	6.37	14.84	7.51	56.30	15.76	18.15
$J = 2.0J_0$	28.23	11.01	12.08	65.15	12.09	19.68
$\psi_f = 1.0\psi_0$	21.12	16.02	5.61	54.84	18.04	16.20
$\psi_f = 0.75\psi_0$	10.93	18.35	6.97	55.28	20.80	17.81
$\psi_f = 0.5\psi_0$	28.64	26.55	12.06	66.03	27.62	20.37
T_L= 2 (N·m)	21.12	16.02	5.61	54.84	18.04	16.20
T_L= 3 (N·m)	21.12	25.84	5.24	54.84	27.58	6.91
T_L= 4 (N·m)	21.12	46.00	4.11	54.84	46.33	7.17

A= Over-Shoot (r/min); B= Speed Drop (r/min); C= Settling Time(ms).

d-axis current set to 0, q-axis current directly output from the controller. The simulation results as shown in Fig. 6. As k_3 increases, speed drop and settling time decrease, indicating an improvement in the system's disturbance rejection performance. However, this comes at the cost of increased overshoot and the steady-state error. In conclude the $(1 + k_3|x_2|)$ can effectively mitigate lumped disturbances, but the numerical value needs to be carefully chosen to avoid sacrificing system performance.

B. Experiment Verification

To further verify the effectiveness of the proposed method, experimental verification of the proposed E-SMC method was conducted of using a comprehensive experimental platform for motor speed regulation and loading. The motor parameters used in the experimental platform as given in Table IV.

The experimental platform mainly consists of the dSPACE MicroLabBox1202 controller as the main controller, the Servo driver, the motor speed encoder, the drive motor, the load motor as load disturbance introduced device, the monitoring computer

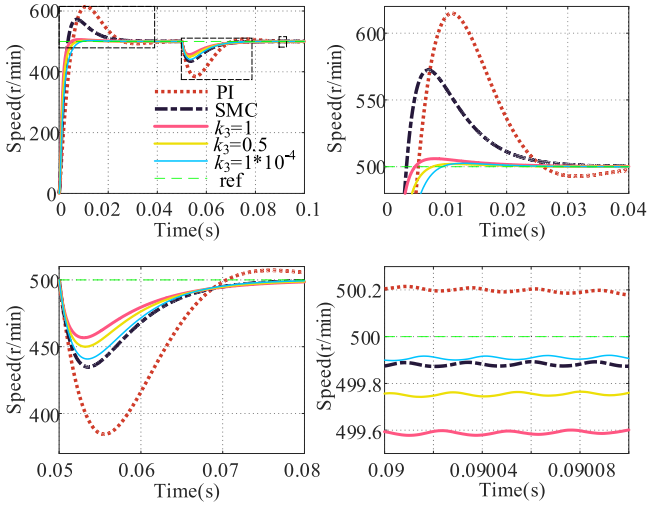

Fig. 6. Speed responses with different value of k_3.

TABLE IV
MAIN PARAMETERS OF THE EXPERIMENTAL SETUP

Parameters	Value
Motor power	0.75 kW
Rated torque	2.39 N·m
Rated current	4.4 A
Rated speed	3000 r/min
Inertia of drive motor	1.59*10^{-4} kg·m^2
Inertia of load motor	12.6*10^{-4} kg·m^2
Transmission stiffness	570 N·m/rad
Encoder resolution	24 bit

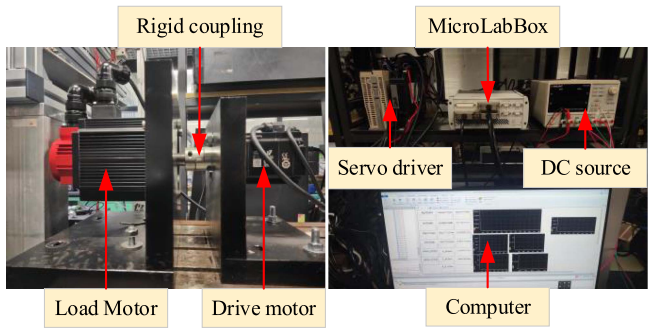

Fig. 7. Experimental platform of motor speed control.

for monitoring feedback values, parameter adjustments, and control signal settings, and the necessary power distribution lines. The experimental platform is shown in Fig. 7.

In the experimental verification, the motor will initially start and run smoothly at 300 r/min for 1.5 s. Then, the speed will be adjusted to 400 r/min and maintained for 2 s, finally the speed will be adjusted back to 300 r/min and run for a further 1.5 s. In the second case, the motor speed will be set and maintained at 300 r/min for 2.5 s. After that, a sudden load disturbance will be added for 1 second and then removed. The load motor will apply this load disturbance, approximately 10% of the rated torque of the load motor.

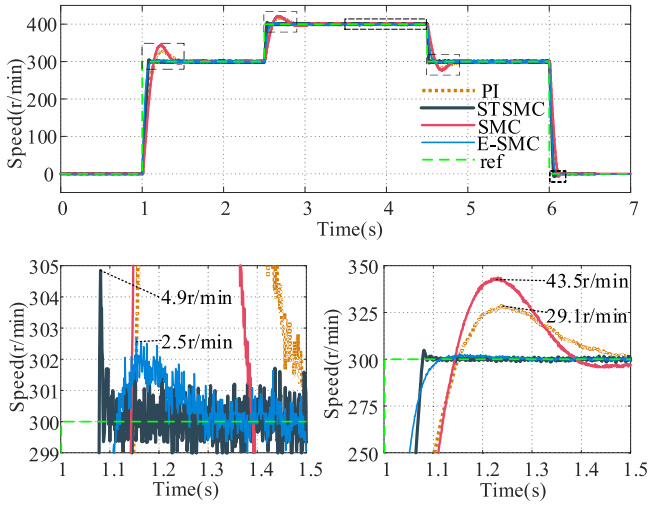

Fig. 8. Speed curves of speed tracking experiments.

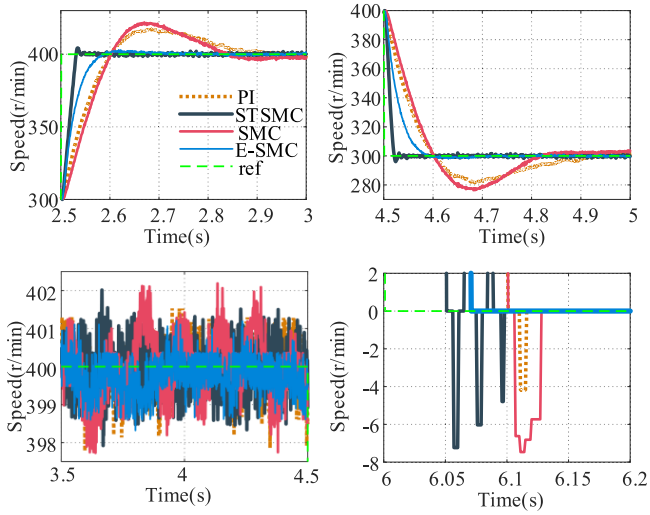

Fig. 9. Speed curves of speed tracking experiments (zoomed).

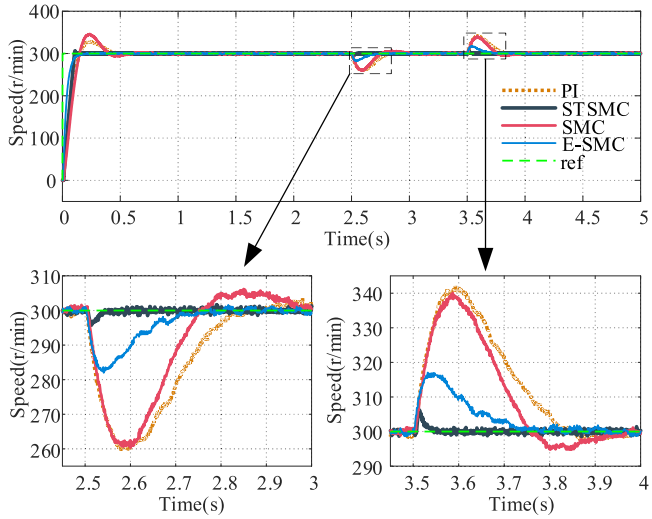

Fig. 10. Speed curves of loading and unloading experiments.

TABLE V
PERFORMANCE COMPARISONS OF CONTROLLERS

Controller	RMS Speed (r/min)	Over-shoot (%)	Speed Drop (%)	Settling Time (ms)
STSMC	0.6392	1.63%	1.75%	107.7
PI	0.6681	9.71%	13.75%	142.4
SMC	0.8542	14.51%	13.37%	136.5
E-SMC	0.5723	0.83%	5.84%	109.1

The supertwisting sliding mode control (STSMC) method is introduced in our experiments for performance comparison with the designed E-SMC. As a representative of second-order SMC, STSMC ensures higher accuracy in tracking performance and simultaneously attenuates the chattering phenomenon [28]. PI controllers and SMC designed based on ERL [25] are compared on the experimental platform to obtain comprehensive analysis and comparison data. The speed curves are recorded respectively as in Figs. 8–10.

From the results of the speed tracking experiments Figs. 8 and 9, The settling times for the E-SMC and traditional SMC systems are 109.6 and 136.5 ms, with overshoot percentages of 14.51% and 0.83%, respectively. The E-SMC system demonstrates precise speed tracking with minimal overshooting. In comparison, the traditional SMC system exhibits some speed fluctuations at different speeds. The PI controller and STSMC have overshoot percentages of 9.71% and 1.63%, with settling times of 142.4 and 107.7 ms, respectively. The performance of the PI controller is comparable to the traditional SMC system, and the performance of E-SMC is comparable to STSMC. However, except for E-SMC, all other controllers experience a reversal phenomenon when the speed returns to zero. In the speed curves analysis from 3.5 to 4.5 s, it can be observed that the speed fluctuation of E-SMC is smaller than that of other controllers. The RMS value of speed tracking error in this period is shown in Table V, with E-SMC at 0.5723, which is 66.9% of SMC and 85.6% of the PI controller, demonstrating the smaller steady-state error of the E-SMC system.

From the results of the load experiments in Fig. 10, the traditional SMC system exhibits significant speed fluctuations of 14.51% on average during load changes. In contrast, the E-SMC system demonstrates much lower speed fluctuations of 5.84%. Additionally, the average speed drop for the PI controller and STSMC is 13.75% and 1.75%, respectively. It can be observed that STSMC shows a significant reduction in speed drop compared to other controllers, indicating STSMC shows greater insensitivity to load disturbances. Through the load experiments, it can be concluded that the E-SMC exhibits faster system response speed and greater insensitivity to load disturbances as compared to the traditional SMC method.

Observing the control input $u(t) = i_q^*$ curve in Fig. 11, where the upper part represents output without loading, and the lower

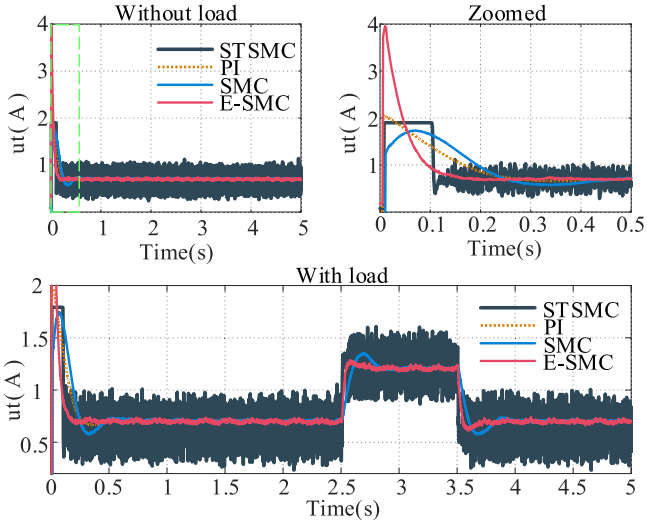

Fig. 11. Control input of different controllers.

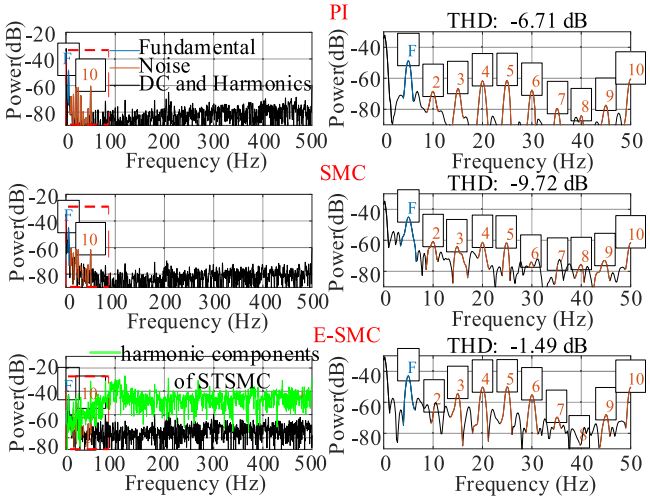

Fig. 12. Harmonic components of controller's input.

part represents output with loading, it can be concluded that E-SMC responds faster and with more precision compared to SMC and PI control input. This is reflected in the better speed tracking performance of the PMSM in the control system. In the case of STSMC, the control input exhibits significant oscillations after reaching steady-state, indicating a chattering phenomenon in the controller. Despite STSMC being a high-order SMC commonly used to reduce chattering [29], in the load experiments also showing strong disturbance rejection, it still exhibits stronger chattering compared to the proposed design in this article. Fig. 12 presents the total harmonic distortion analysis of control input, from top to bottom for PI, SMC, and E-SMC harmonic components. All these three controllers have a fundamental component at 5 Hz, numerically equal to the motor speed of 300 r/min. It can be observed that STSMC shows a significant increase in the power of high-frequency components, indicating that STSMC generates more high-frequency control signals.

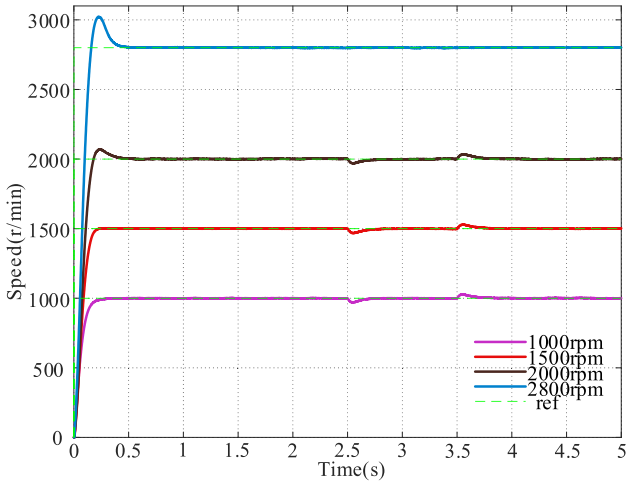

Fig. 13. Speed curves of E-SMC under different reference speeds.

Further analyzing the E-SMC system under higher speeds and increased load, where the load size is half of the rated load of the motor. The speed tracking curve of the PMSM system, controlled by a set of unchanged parameters for the E-SMC, is shown in Fig. 13. The speed tracking curve of the PMSM system is stable in the range of 1000–2000 r/min and exhibits significant overshoot when reaching 3000 r/min. This is due to significant variations in the range of system state variables, requiring adjustments to the controller. It is evident that the E-SMC controller demonstrates good adaptability within a certain range.

In conclusion, the experimental results have verified the feasibility of the E-SMC method, demonstrating its practical applicability and value. The E-SMC system exhibits superior performance in terms of faster dynamic response, suppression of the chattering phenomenon, higher accuracy in speed tracking and good adaptability within a certain range.

V. Conclusion

This article presents a novel ASMRL based on the exponential function was designed and analyzed to accelerates the SMC reaching process and effectively suppress the chattering phenomenon. This method was directly applied to the SMC systems designed based on conventional SMRL to enhance their performance. It is readily applicable to practical industrial systems without additional implementation costs. An enhanced sliding mode controller was developed for the PMSM based on the proposed ASMRL. The effectiveness and superiority of the proposed method were robustly supported by both simulation and experimental results.

References

[1] H. Wang and J. Leng, "Summary on development of permanent magnet synchronous motor," in *Proc. Chin. Control Decis. Conf.*, 2018, pp. 689–693.

[2] X. Wang, M. Reitz, and E. E. Yaz, "Field oriented sliding mode control of surface-mounted permanent magnet AC motors: Theory and applications to electrified vehicles," *IEEE Trans. Veh. Technol.*, vol. 67, no. 11, pp. 10343–10356, Nov. 2018, doi: 10.1109/TVT.2018.2865905.

[3] C. Mu and H. He, "Dynamic behavior of terminal sliding mode control," *IEEE Trans. Ind. Electron.*, vol. 65, no. 4, pp. 3480–3490, Apr. 2018, doi: 10.1109/TIE.2017.2764842.

[4] Y. Feng, X. Yu, and F. Han, "High-order terminal sliding-mode observer for parameter estimation of a permanent-magnet synchronous motor," *IEEE Trans. Ind. Electron.*, vol. 60, no. 10, pp. 4272–4280, Oct. 2013, doi: 10.1109/TIE.2012.2213561.

[5] S. S.-D. Xu, C.-C. Chen, and Z.-L. Wu, "Study of nonsingular fast terminal sliding-mode fault-tolerant control," *IEEE Trans. Ind. Electron.*, vol. 62, no. 6, pp. 3906–3913, Jun. 2015, doi: 10.1109/TIE.2015.2399397.

[6] Weibing Gao and J. C. Hung, "Variable structure control of nonlinear systems: A new approach," *IEEE Trans. Ind. Electron.*, vol. 40, no. 1, pp. 45–55, Feb. 1993, doi: 10.1109/41.184820.

[7] A. K. Junejo et al., "Novel fast terminal reaching law based composite speed control of PMSM drive system," *IEEE Access*, vol. 10, pp. 82202–82213, 2022, doi: 10.1109/ACCESS.2022.3196785.

[8] X. Zhang, L. Sun, K. Zhao, and L. Sun, "Nonlinear speed control for PMSM system using sliding-mode control and disturbance compensation techniques," *IEEE Trans. Power Electron.*, vol. 28, no. 3, pp. 1358–1365, Mar. 2013, doi: 10.1109/TPEL.2012.2206610.

[9] H. Wang et al., "Continuous fast nonsingular terminal sliding mode control of automotive electronic throttle systems using finite-time exact observer," *IEEE Trans. Ind. Electron.*, vol. 65, no. 9, pp. 7160–7172, Sep. 2018, doi: 10.1109/TIE.2018.2795591.

[10] T. Li, Y. Zhao, and L. Hou, "Adaptive sliding mode control with disturbance observer for speed regulation system of permanent magnet synchronous motor," *IEEE Access*, vol. 11, pp. 17021–17030, 2023, doi: 10.1109/ACCESS.2023.3245635.

[11] A. K. Junejo, W. Xu, C. Mu, M. M. Ismail, and Y. Liu, "Adaptive speed control of PMSM drive system based a new sliding-mode reaching law," *IEEE Trans. Power Electron.*, vol. 35, no. 11, pp. 12110–12121, Nov. 2020, doi: 10.1109/TPEL.2020.2986893.

[12] D. Zhang et al., "A PMSM control system for electric vehicle using improved exponential reaching law and proportional resonance theory," *IEEE Trans. Veh. Technol.*, vol. 72, no. 7, pp. 8566–8578, Jul. 2023, doi: 10.1109/TVT.2023.3236628.

[13] D. Tian, R. Xu, E. Sariyildiz, and H. Gao, "An adaptive switching-gain sliding-mode-assisted disturbance observer for high-precision servo control," *IEEE Trans. Ind. Electron.*, vol. 69, no. 2, pp. 1762–1772, Feb. 2022, doi: 10.1109/TIE.2021.3057004.

[14] S. Li, M. Zhou, and X. Yu, "Design and implementation of terminal sliding mode control method for PMSM speed regulation system," *IEEE Trans. Ind. Informat.*, vol. 9, no. 4, pp. 1879–1891, Nov. 2013, doi: 10.1109/TII.2012.2226896.

[15] B. Xu, L. Zhang, and W. Ji, "Improved non-singular fast terminal sliding mode control with disturbance observer for PMSM drives," *IEEE Trans. Transp. Electrific.*, vol. 7, no. 4, pp. 2753–2762, Dec. 2021, doi: 10.1109/TTE.2021.3083925.

[16] J. Song, Y. Niu, and Y. Zou, "Finite-time stabilization via sliding mode control," *IEEE Trans. Autom. Control*, vol. 62, no. 3, pp. 1478–1483, Mar. 2017, doi: 10.1109/TAC.2016.2578300.

[17] Y. Wang, Y. Feng, X. Zhang, and J. Liang, "A new reaching law for antidisturbance sliding-mode control of PMSM speed regulation system," *IEEE Trans. Power Electron.*, vol. 35, no. 4, pp. 4117–4126, Apr. 2020, doi: 10.1109/TPEL.2019.2933613.

[18] L. Xiong, J. Wang, X. Mi, and M. W. Khan, "Fractional order sliding mode based direct power control of grid-connected DFIG," *IEEE Trans. Power Syst.*, vol. 33, no. 3, pp. 3087–3096, May 2018, doi: 10.1109/TPWRS.2017.2761815.

[19] X. Gao, Z. Ren, L. Zhai, Q. Jia, and H. Liu, "Two-stage switching hybrid control method based on improved PSO for planar three-link underactuated manipulator," *IEEE Access*, vol. 7, pp. 76263–76273, 2019, doi: 10.1109/ACCESS.2019.2921968.

[20] J. Min, Y. Fang, and Z. Xu, "Adaptive fast terminal sliding mode control for a class of uncertain system," in *Proc. Int. Conf. Ind. Inf. Syst.*, 2009, pp. 337–340.

[21] H. Komurcugil, S. Bayhan, N. Guler, and H. Abu-Rub, "A new exponential reaching law approach to the sliding mode control: A multilevel multifunction converter application," *IEEE Trans. Ind. Electron.*, vol. 70, no. 8, pp. 7557–7568, Aug. 2023, doi: 10.1109/TIE.2022.3229369.

[22] V. I. Utkin, "Sliding mode control design principles and applications to electric drives," *IEEE Trans. Ind. Electron.*, vol. 40, no. 1, pp. 23–36, Feb. 1993, doi: 10.1109/41.184818.

[23] L. Hou, J. Ma, and W. Wang, "Sliding mode predictive current control of permanent magnet synchronous motor with cascaded variable rate sliding mode speed controller," *IEEE Access*, vol. 10, pp. 33992–34002, 2022, doi: 10.1109/ACCESS.2022.3161629.

[24] A. Wang and S. Wei, "Sliding mode control for permanent magnet synchronous motor drive based on an improved exponential reaching law," *IEEE Access*, vol. 7, pp. 146866–146875, 2019, doi: 10.1109/ACCESS.2019.2946349.

[25] C. J. Fallaha, M. Saad, H. Y. Kanaan, and K. Al-Haddad, "Sliding-mode robot control with exponential reaching law," *IEEE Trans. Ind. Electron.*, vol. 58, no. 2, pp. 600–610, Feb. 2011, doi: 10.1109/TIE.2010.2045995.

[26] Y. X. Su, C. H. Zheng, and B. Y. Duan, "Automatic disturbances rejection controller for precise motion control of permanent-magnet synchronous motors," *IEEE Trans. Ind. Electron.*, vol. 52, no. 3, pp. 814–823, Jun. 2005, doi: 10.1109/TIE.2005.847583.

[27] A. Lidozzi, V. Serrao, L. Solero, F. Crescimbini, and A. Di Napoli, "Direct tuning strategy for PMSM drives," in *Proc. IEEE Ind. Appl. Soc. Annu. Meeting*, 2008, pp. 1–7, doi: 10.1109/08IAS.2008.177.

[28] Q. Hou and S. Ding, "GPIO based super-twisting sliding mode control for PMSM," *IEEE Trans. Circuits Syst. II, Exp. Briefs*, vol. 68, no. 2, pp. 747–751, Feb. 2021, doi: 10.1109/TCSII.2020.3008188.

[29] J. Gil, S. You, Y. Lee, and W. Kim, "Super twisting-based nonlinear gain sliding mode controller for position control of permanent-magnet synchronous motors," *IEEE Access*, vol. 9, pp. 142060–142070, 2021, doi: 10.1109/ACCESS.2021.3121127.

[30] V. Utkin, "Variable structure systems with sliding modes," *IEEE Trans. Autom. Control*, vol. 22, no. 2, pp. 212–222, Apr. 1977, doi: 10.1109/TAC.1977.1101446.

Zhang Zhang received the B.S. degree in automation from the University of South China, Hengyang, China, in 2022. He is currently working toward the master degree in control engineering with the College of Mechatronics and Control Engineering, Shenzhen University, Shenzhen, China.

His current research interests include the servo motor drive and control and sliding mode control.

Xiaodong Yang received B.S degree in electrical engineering from Henan Institute of Science and Technology, Henan, China, in 2020. He is currently working toward the master degree in control engineering with the College of Mechatronics and Control Engineering, Shenzhen University, Shenzhen, China.

His research interests include wireless power transfer, dc–dc converter, and control theory.

Weiyu Wang (Student Member, IEEE) is currently working toward the Ph.D. degree in electrical engineering with the Department of Electrical Engineering, Hong Kong Polytechnic University, Hong Kong.

His research interests include electrical machine drive and position-sensorless drive.

Kaiwen Chen (Member, IEEE) was born in Zhejiang, China. He received the B.Eng. degree from Harbin Institute of Technology, China, in 2016, and M.Sc. and Ph.D. degrees from Hong Kong Polytechnic University, Hong Kong, in 2017 and 2022, respectively.

His main research interests include wireless power transfer, electric vehicles, control theory and artificial intelligence.

Norbert Chow Cheung (Senior Member, IEEE) received the B.Sc. degree from Queen Marry College, London University, London, U.K., the M.Sc. degree from the University of Hong Kong, Hong Kong, and the Ph.D. degree from the University of New South Wales, Sydney, NSW, Australia, in 1981, 1987 and 1996, respectively.

He is currently with the College of Mechatronics and Control Engineering, Shenzhen University, Shenzhen, China. His research interests include actuators design, motion control, and robotics.

Jianfei Pan (Member, IEEE) received the Ph.D. degree from the Department of Electrical Engineering, The Hong Kong Polytechnic University, Hong Kong, Hong Kong, in 2006.

He is currently with the College of Mechatronics and Control Engineering, Shenzhen University, Shenzhen, China. His main research interest includes the design and control of linear motors and generators.